Modeling of alkali metal release during biomass pyrolysis

Hesameddin, Fatehi; Li, Z. S.; Bai, X. S.; Aldén, M.

Published in:
Proceedings of the Combustion Institute

DOI:
10.1016/j.proci.2016.06.079

2017

Title page:

Modeling of Alkali Metal Release during Biomass Pyrolysis

H. Fatehi[*,1], Z.S. Li[2], X.S. Bai[1], M. Aldén[2]

[1]Division of Fluid Mechanics, Lund University, 22100, Lund, Sweden

[2]Division of Combustion Physics, Lund University, 221 00 Lund, Sweden

This is the peer reviewed version of the following article: [H. Fatehi, Z.S. Li, X.-S. Bai, M. Aldén, *'Modeling of Alkali Metal Release during Biomass Pyrolysis'*, **Proc. Combust. Inst. 36**, 2243-2251 **(2017)**.], which has been published in final form at [DOI: 10.1016/j.proci.2016.06.079].

Modeling of Alkali Metal Release during Biomass Pyrolysis

H. Fatehi[*,1], Z.S. Li[2], X.S. Bai[1], M. Aldén[2]

[1]Division of Fluid Mechanics, Lund University, 22100, Lund, Sweden

[2]Division of Combustion Physics, Lund University, 221 00 Lund, Sweden

[*]Corresponding author:

Hesameddin Fatehi
Division of Fluid Mechanics
Department of Energy Sciences
Lund University,
P.O. Box 118, SE-22100 Lund
Sweden
Email: Hesameddin.fatehi@energy.lth.se
Fax: +46-46-222 4717

Colloquium: Solid Fuel Combustion

Word counts by method 1:	**5778**
Main Text:	**3607**
Equations:	**190**
References:	**507**
Tables:	**297 (Table: 69+228)**
Figures:	**1177 (Figs: 118+111+228+103+325+292)**

Abstract

The release of alkali metals during biomass pyrolysis was numerically and experimentally studied. The concentration of sodium and potassium in the gas phase above a biomass particle was measured; quantitative and time resolved data was acquired by means of the Laser-Induced Breakdown Spectroscopy (LIBS) technique. LIBS made it possible to extend the measurements of alkali metal concentration to the sooty pyrolysis stage. Data from the measurements revealed a staged release of alkali metals from biomass. Two distinct peaks of concentrations were observed, one associated with the pyrolysis stage and the other with the gasification stage. Since during the pyrolysis stage a large temperature gradient exist inside the particle, numerical simulations were carried out to explain the experimental measurements and extract the kinetic data. Using a detailed particle model, the rates of potassium and sodium release from the particle during the pyrolysis stage were attained. For sodium release the activation energy was found to be in the range of 218 to $248\ kJ/mole$ and for potassium release it was found to be between 168 and $198\ kJ/mole$. Furthermore, equilibrium calculations were performed to identify the stable sodium and potassium compounds and their phases during the pyrolysis stage of the particle.

Keywords: Alkali metal release; Biomass; Pyrolysis; LIBS; In situ measurement

1. Introduction

Owing to the presence of high amount of alkali metals (potassium and sodium) in some biomass sources, the release of alkali metals during biomass pyrolysis and gasification can cause serious damage to the gasification systems. The problems can lead to reduced heat transfer, disturbance of the gas flow, physical damage to the gasifier parts, corrosion and erosion of the parts due to fouling, slagging, and

agglomeration [1-5]. To prevent the damage caused by these species it is important to understand the release of alkali metals during thermochemical conversion of biomass.

Recent studies identified staged release of sodium and potassium from biomass during the biomass pyrolysis stage and the char gasification/combustion stage [6, 7]. During these different stages, the composition of potassium and sodium compounds can be different. Potassium in biomass is mostly in the form of ionic salts [3, 8] and depending on the presence of water vapor, the main form of potassium compound in gas phase can change between KOH and KCl [3]. Sodium in biomass usually exists at lower concentration compared with potassium and behaves similarly as potassium. Sodium compounds in the gas phase are mostly NaCl and NaOH [8]. Sodium can also react with sulfur to form sulfates. Cl and S can assist the mobility of sodium and potassium; however, there are studies showing that Cl and S can be released at low temperature, between 200-700 °C, while the potassium content of biomass remains intact at these temperatures [9-12]. While the main Cl compounds at low temperature are HCl and methyl chloride (CH_3Cl) [10, 13], at temperatures higher than 700 °C, Cl will be released mainly in the form of alkali metal chlorine [14]. More release of sodium compared with potassium has been reported at low temperature pyrolysis [15]. The higher release of sodium at temperature below 700 °C can be associated with the sublimation of NaCl, while the sublimation of KCl will occur at temperatures higher than 700 °C [15]. Part of the potassium release during pyrolysis can be redeposited as discrete particles of KCl and K_2CO_3 bounded to the organic matrix of biomass. Later in the process at higher temperatures, the initial release of potassium to the gas phase is due to the sublimation of these discrete KCl particles [11]. By increasing the temperature, it was shown that the release of K will increase [16, 17].

Above mentioned studies show that there is a strong dependency between the amount and composition of alkali metals compounds with temperature, gas composition and the stage of biomass conversion. Despite these efforts, qualitative and time resolved data on the gas phase concentrations and

release kinetics of alkali metals during biomass pyrolysis is rare. The focus of this paper is on the release of sodium and potassium during the pyrolysis stage of biomass at different temperatures. To this aim, a joined experimental and numerical study was performed. Experimental data was attained by placing a biomass particle in the hot flue gas of a methane flame and Laser-Induced Breakdown Spectroscopy (LIBS) was employed to measure the time-resolved concentration of potassium and sodium at the boundary of the particle at different temperatures and gas compositions. The LIBS method has the advantage of providing in-situ and time resolved data during the sooty pyrolysis stage, while other techniques may fail due to the laser scattering in this condition. Previous studies on the release of sodium from a coal particle with planar laser-induced fluorescence (PLIF) [7, 18] was limited to the combustion and gasification stage due to the high level of laser scattering during the pyrolysis stage. A recent study on release of potassium from a pine wood particle by LIBS technique has also shown the capability of the technique for quantitative measurement of alkali metal release [19]. The experimental data is used in a detailed numerical model of the particle to estimate the chemical kinetics of alkali metals release. Furthermore, the kinetic data was supplemented by equilibrium calculations to study the stable species in the gas phase under the experimental condition.

2. Experimental measurements

The LIBS technique was adopted to measure quantitatively the concentration of alkali metals during thermochemical conversion of biomass. LIBS provides high temperature plasma using a high energetic laser pulse. The existing species in the focus point of the laser are dissociated to atoms and the excited atoms will deliver a spectral signature that can be detected by a spectrometer and can be calibrated to provide quantitative data of the element concentration. By employing the LIBS technique, temporal release of potassium and sodium was measured in the flue gas of methane combustion with different

concentrations of O_2, diluted by carbon dioxide, at four different temperatures. The hot flue gas was provided from a laminar multi-jet burner flame.

The particle samples were cylindrical pellets from Swedish wood with a diameter of 8 mm and height of 4 mm. The ultimate analysis of the samples shows 50.6% C, 6.6% H and 42.8% O on dry ash free basis. The mass fraction of sodium and potassium in the dry particle are 0.03% and 0.05%, respectively. The details of the experimental set-up and the measurement technique can be found in [6]. The experimental conditions are presented in Table 1. Two equivalence ratios, ϕ, and four different temperatures are studied. Temperatures at the exit plane of the burner at three locations, center, middle and outer limit, are presented in the table.

Table 1. Temperature profile along the radius of the burner exit plane for various test cases

ϕ	Temperature profile along radius [K]			Label
	r=0	r=20mm	r=33mm	
0.9	1596	1515	577	F1
	1483	1272	562	F2
	1408	1100	567	F3
1.2	1518	1491	718	F4

3. Numerical analysis

During the pyrolysis stage, the particle experiences a large temperature gradient from its surface to its center. This is due to the fact that the particle is thermally thick and is still in the transient heating up stage. Due to the limitation in the experiment, the detailed information inside the particle is not available. To relate the measurement data to the processes inside the particle during this transient stage, a detailed numerical model was employed. The particle domain is discretized into control volumes and mass, species and energy conservation equations are solved for each control volume. The model considers the convective and conductive heat and mass transfer and radiative heat transfer inside the

particle as well as heat and mass transfer between the particle and the surrounding gas. The particle model is presented in [20]. A sub-model is developed to calculate the release rate of alkali metals based on the measured concentrations. This sub-model is presented below.

3.1. Alkali metal release sub-model

Considering the convective and diffusive transport of a given species from the porous structure of biomass to the ambient, the total mass flux of a given species j can be represented as follows [21],

$$\dot{m}_j = Y_j^s \sum_j \dot{r}_j + A_P h_m \rho_g (Y_j^\infty - Y_j^s), \tag{1}$$

where Y_j is the mass fraction of species j and the superscripts s and ∞ represent the conditions at the particle surface and in the ambient gas, respectively. ρ_g is the gas density and A_P is the outer surface area of the particle which changes with time due to the particle shrinkage and h_m is the mass transfer coefficient. In this equation, the diffusion through the ash layer is neglected due to the low ash content of the particle. By dividing the particle into control volumes where i represents each control volume cell inside the particle, $\dot{r}_j = \sum_i \Re_{j,i} V_i$ is the sum of the formation/consumption rates of species j in the entire particle domain. $\Re_j$ is the volumetric formation/consumption rate of mass of species j where O_2, CO_2, H_2O, CH_4, H_2, Tar, K and Na are considered and V_i is the volume of the cell i. The rates of formation/consumption of each species due to various processes inside the particle are presented as follows:

$$\begin{aligned}
\Re_{\mathrm{H2O}} &= \Re_m + \vartheta_{\mathrm{H2O}} \Re_g - M_{\mathrm{H2O}}/M_{\mathrm{c}} \Re_{c_{\mathrm{H2O}}} \\
\Re_{\mathrm{CO2}} &= \vartheta_{\mathrm{CO2}} \Re_g - M_{\mathrm{CO2}}/M_{\mathrm{c}} \Re_{c_{\mathrm{CO2}}} \\
\Re_{\mathrm{CO}} &= \vartheta_{\mathrm{CO}} \Re_g + M_{\mathrm{CO}}/M_{\mathrm{c}} \left(\Re_{c_{\mathrm{O2}}} + 2\Re_{c_{\mathrm{CO2}}} + \Re_{c_{\mathrm{H2O}}} \right) \\
\Re_{\mathrm{CH4}} &= \vartheta_{\mathrm{CH4}} \Re_g
\end{aligned} \tag{2}$$

$$\Re_{\mathrm{H2}} = \vartheta_{\mathrm{H2}} \Re_g + M_{\mathrm{H2}}/M_{\mathrm{c}}\, \Re_{c_{\mathrm{H2O}}}$$

$$\Re_{\mathrm{O2}} = -2\, M_{\mathrm{O2}}/M_{\mathrm{c}}\, \Re_{c_{\mathrm{O2}}},$$

where $\Re_m$ is the moisture evaporation rate, $\Re_g$ is the rate of formation of gas due to pyrolysis and $\Re_c$ is the rate of heterogeneous reactions of char with O_2, CO_2 and H_2O. ϑ_j accounts for the mass fraction of species j on the basis of the total gas produced due to pyrolysis and M_j is the molar mass of species or element j. The mass fraction of each species at the particle surface can be obtained by dividing the mass flux of species j by sum of all the species mass fluxes,

$$Y_j^s = \frac{\sum_i \Re_{j,i} V_i + A_P h_m \rho_g Y_j^\infty}{\sum_j \sum_i \Re_{j,i} V_i + A_P h_m \rho_g}. \tag{3}$$

The first term in the numerator is the total mass formation/consumption rates of species j in the entire particle volume due to moisture evaporation, pyrolysis and heterogeneous reactions. The second term in the numerator is the mass transfer of species j from/to the ambient gas. The two terms in the denominator are the sum of all the species mass fluxes at the particle surface.

Equation (3) provides the connection between the rate of release of potassium and sodium from the particle and the measured concentrations at the particle surface. In the experiments, the elemental concentrations of potassium, C_{K}^{Exp}, were measured. The mass fraction of potassium is equal to the concentration divided by the gas density, $Y_{\mathrm{K}}^{Exp} = C_{\mathrm{K}}^{Exp}/\rho_g$. Due to the short distance between the particle surface and the measurement point the mass fraction of potassium at the measurement point is approximately equal to the mass fraction at the particle surface, $Y_{\mathrm{K}}^s \cong Y_{\mathrm{K}}^{Exp}$ and similarly for sodium, $Y_{\mathrm{Na}}^s \cong Y_{\mathrm{Na}}^{EXP}$.

3.2. Extracting kinetic data

For all the species in the system, except for K and Na, the formation and consumption rates are known, cf, Eq. (2). By rearranging Eq. (3) and assuming that the concentrations of the gaseous potassium and sodium in the ambient gas are zero, the rate of release of potassium and sodium are,

$$\dot{r}_k = \frac{Y_k^s\left(\sum_{j\neq k}\dot{r}_j + A_P h_m \rho_g\right)}{1 - Y_k^s}\,, k = \text{K and Na.} \tag{4}$$

The rates of formation of K_g and Na_g are equal to the rates of consumption of corresponding species in solid form inside the particle. If $m_{\mathrm{K}_{solid}}$ and $m_{\mathrm{Na}_{solid}}$ represent the time dependent mass of K and Na that remain inside the particle, by assuming a first order kinetic rate for consumption of solid K and Na, one can write,

$$\begin{aligned}\frac{dm_{\mathrm{K}_{solid}}}{dt} &= m_{\mathrm{K}_{solid}} A_{\mathrm{K}}\, exp\left(-\frac{E_{\mathrm{K}}}{\mathcal{R}T}\right) = \dot{r}_{\mathrm{K}} \\ \frac{dm_{\mathrm{Na}_{solid}}}{dt} &= m_{\mathrm{Na}_{solid}} A_{\mathrm{Na}} exp\left(-\frac{E_{\mathrm{Na}}}{\mathcal{R}T}\right) = \dot{r}_{\mathrm{Na}},\end{aligned} \tag{5}$$

where A is the pre-exponential factor, E is activation energy and $\mathcal{R}$ is the universal gas constant. The kinetic constant for potassium and sodium release can be obtained by knowing the instantaneous consumption rates and masses of K and Na ($\frac{\dot{r}_{\mathrm{K}}}{m_{\mathrm{K}_{solid}}}$ and $\frac{\dot{r}_{\mathrm{Na}}}{m_{\mathrm{Na}_{solid}}}$) and the particle temperature. The release rates of K and Na ($\dot{r}_k$) are calculated by using the experimental data and Eq. (4) while the particle temperature and the instantaneous masses of K and Na are obtained from the detailed particle model. Linear least-square fitting in $\ln\left(\frac{\dot{r}_k}{m_{k_{solid}}}\right)$ and $\frac{1}{T}$ space then provides the estimate of A and E through rearrangement of Eq. (5).

4. Results and discussions

4.1. Kinetic rate constants of alkali metal release

The temperature inside the particle shows a high spatial variation during the pyrolysis stage due to the large Biot number and the importance of the intra-particle heat transfer. The particle model showed that this variation can be up to several hundred Kelvin and therefore it is not suitable to assign an average temperature to the particle while calculating the kinetic rate constants of alkali metal release. Figure 1 shows the particle temperature history during the pyrolysis stage. The difference between the highest (at the surface) and lowest (at the center) temperature in the particle is also presented in the figure. The temperature difference reaches to 500 K during a large part of the pyrolysis stage.

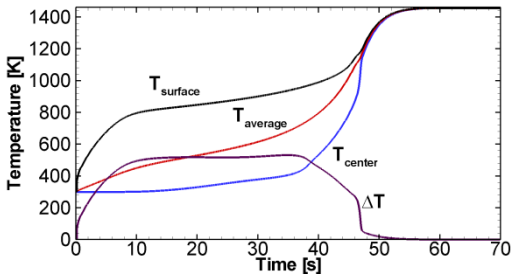

Figure 1. Particle temperature at surface and center, average temperature and temperature difference during the pyrolysis stage

To assign the corresponding temperature to the release rates, both distributions of temperature and the rates are required. The temperature distribution inside the particle at each time during the particle conversion can be calculated from the particle model. Since $\dot{r}_k = \sum_i \Re_{k,i} V_i$, the distribution of the $\Re_{k,i}$ inside the particle is required to be assigned to the correct temperature. To find a spatial distribution for $\Re_{k,i}$, it is assumed that the K and Na release start from the particle surface, similar to the drying and pyrolysis processes, and also the spatial distribution of the K and Na release rate inside the particle is similar to that of the pyrolysis rate. Figure 2 shows the spatial distribution of the pyrolysis rate at

different times between t = 10 and 50 s. At the beginning of the process, the distribution is more spread along the particle radius and shows a smaller peak value due to the relatively lower particle temperature. When the particle temperature increases, the distribution becomes narrower, representing a sharper pyrolysis front. The same spatial distribution as presented in Figure 2 is assigned to release of K and Na providing the location of the reaction front inside the particle. By knowing the location of the reaction front at any time, a temperature distribution can be associated to the release rates.

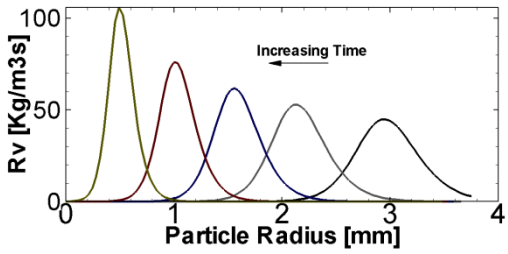

Figure 2. Spatial distribution of pyrolysis rate inside the particle at different time instances

By plotting $\ln(\dot{r}_k/m_{k_{solid}})$ versus $1000/T$ and fitting a linear regression function to the data points, estimates of $E_k/\mathcal{R}$ and $\ln(A_k)$ can be obtained. Figure 3 shows the scatter plots of the inverse temperature and the natural logarithm of the release rates for both K and Na during the pyrolysis stage. Each data point in this figure represents a numerical cell with nonzero release rate at each time step for all four cases, **F1-F4**. The linear fit to each set of data, **F1** to **F4**, is presented with a solid line in the same figure. The activation energy is equal to the slope of the linear regression times the universal gas constant, $\mathcal{R}$. For sodium release, the activation energy spans from 218 to 248 $kJ/mole$ and for potassium release it changes between 168 and 198 $kJ/mole$. The pre-exponential factor is equivalent to the exponent of y intercept and shows values between 10^{12}~10^{14} $1/s$ for sodium and 4×10^{9}~9×10^{10} $1/s$ for potassium. By fitting a line to all data sets, the average values of activation energies and pre-exponential factors for sodium and potassium release during the pyrolysis stage can be obtained,

$$A_{\mathrm{K}} = 5.3 \times 10^{10}\ 1/s\ ;\ E_{\mathrm{K}} = 185\ kJ/mole$$
$$A_{\mathrm{Na}} = 3 \times 10^{12}\ 1/s\ ;\ E_{\mathrm{Na}} = 223\ kJ/mole. \quad (6)$$

During calculation of the activation energies and pre-exponential factors for the release rate of sodium and potassium, the data corresponding to low temperatures (less than 750 K) were excluded, as they showed very low activation energies. The release of potassium and sodium at low temperature can be due to the sublimation of water solvable compounds which is controlled by the heat transfer rate rather than the kinetic rate.

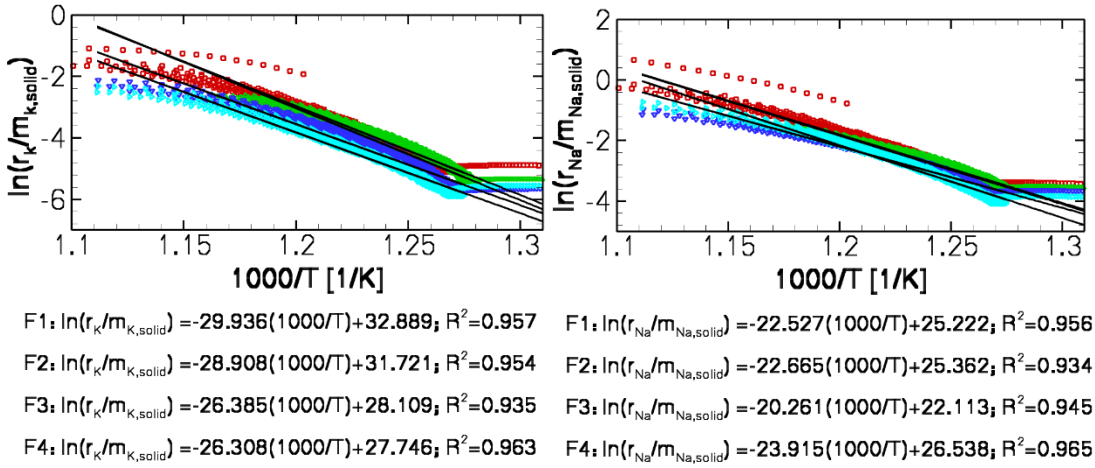

Figure 3. Scatter plot of the natural logarithm of $\dot{r}_k/m_{k_{solid}}$ versus the inverse of temperature for sodium and potassium during the pyrolysis stage

Figure 4 shows the normalized mass of sodium and potassium in the biomass during the pyrolysis stage. The mass is normalized with the initial mass of each of these species inside the solid structure, as reported in the ultimate analysis of the particle. The sodium mass curves show that up to 55% of the sodium is released during the pyrolysis stage. This value for potassium is much lower, up to 10%,

showing that the potassium release mostly occurs during the char burning and ash-cooking stages at higher temperatures. This is in agreement with the findings of previous studies, e.g., [15], where the release of potassium was reported to occur at higher temperature compared with that of sodium.

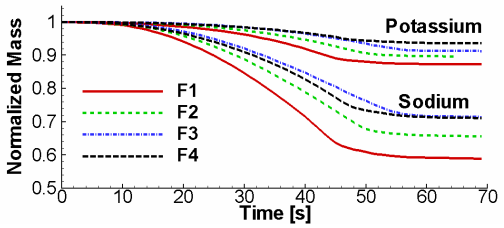

Figure 4. Normalized mass of sodium and potassium in the particle during the pyrolysis stage

The measured concentrations of K and Na for the four cases, **F1-F4**, during the pyrolysis stage along with the model predictions are presented in Figure 5. Each measurement point is an average of data from ten different biomass samples. The peaks of the sodium and potassium release correspond to the highest particle mass loss rate. While the model can predict the peak of sodium and potassium release and the trend regarding different cases, there is a discrepancy between the measurements and the model prediction at the early stage of the process. This early stage corresponds to the sodium and potassium release at low temperature, for which the data was disregarded when estimating the kinetic constants. The larger difference between model prediction and measurement in the case of sodium compared with potassium is due to the lower sublimation temperature of NaCl compared with KCl [15] and higher release of Na at lower temperature. The kinetic constants for release of potassium during the char combustion and ash-cooking stages along with a proposed mechanism are presented in [6].

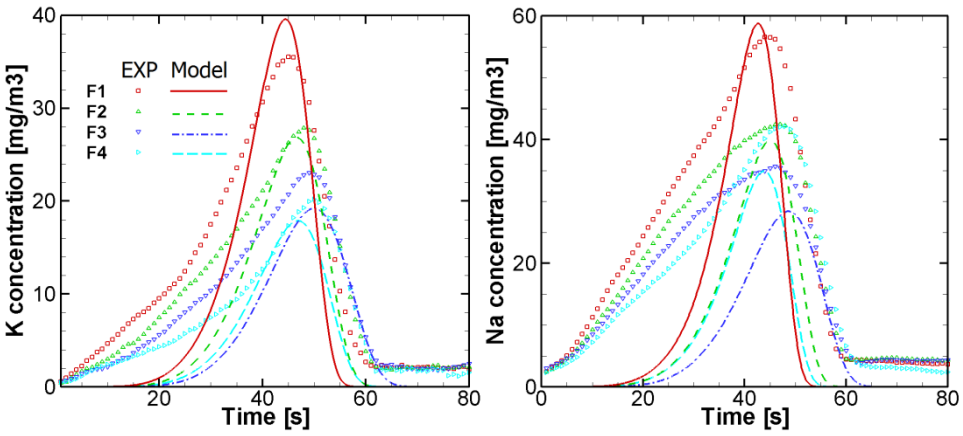

Figure 5. Measurements and model prediction of mass concentration of potassium and sodium at four different flame conditions; symbols are from the experiment and lines are from the numerical model

4.2. Thermodynamic equilibrium calculations

The data from the LIBS measurement can provide the total atomic release of potassium and sodium from the particle. However, the different species that contain potassium and sodium cannot be identified by this technique. The knowledge of the gas phase composition is essential, as some of the species are more likely to cause problems such as slagging than the others. To investigate the stable species in the gas phase under the experimental conditions, thermodynamic equilibrium calculations were carried out. In equilibrium calculations, for a given composition, temperature and pressure of the system, the stable species and their state are identified by minimizing the total Gibbs free energy of the system while maintaining the mass conservation constraint. The calculations are performed under the assumption that the residence time of the system is significantly longer than the chemical kinetic time scale and all the species are homogenously mixed and available for reaction [22]. Thus, the results can be considered qualitative and serves as a reference.

The equilibrium calculations were performed using CHEMKIN [23]. More than 100 species were considered in the system. The list of elements and species used in the calculations are presented in Table 2. The thermodynamic data for the listed species are from Goos et al. [24] and the CHEMKIN database [23]. For some of the potassium compounds which weren't available in those databases, thermodynamic

data from Glarborg and Marshall [25] was used. Thermodynamic properties of K_2O-(SiO_2) and Na_2O-(SiO_2) systems were extracted from Allendorf and Spear [26].

Table 2. List of elements and species included in the equilibrium calculations

Elements	Species in gas, liquid and solid phases
C, H, O, N	Biomass (approximated by $C_6H_{10}O_5$), Char (Approximated by $C_{(S)}$), CH_4 C_2H_2 C_2H_4 CO CO_2 $H_2O_{(L)}$ H_2O H_2 O O_2 O_3 OH NH NH_2 NH_3 N_2H_4 HCN HNO HNO_2 HNO_3 N_2 N_2O N_2O_4 NO NO_2
K	K KOH $(KOH)_2$ $K_2CO_{3(S)}$ $K_2O_{(S)}$ KO KO_2 KCl $KCl_{(L)}$ $KCl_{(S)}$ $(KCl)_2$ KSO_2 KSO_3 $KHSO_4$ $KHSO_3$ KSO_4 KSO_3CL K_2SO_4 $K_2SO_{4(S)}$ $(K_2SO_4)_2$ $(K_2SO_4)_3$ $(K_2SO_4)_4$ $K_2SO_{4(L)}$ $K_2O.(SiO_2)$ $K_2O.(SiO_2)_2$ $K_2O.(SiO_2)_4$ $K_2O.(SiO_2)_{(S)}$ $K_2O.(SiO_2)_{2(S)}$ $K_2O.(SiO_2)_{4(S)}$ KCN
Na	Na $Na_2O_{(S)}$ Na_2SO_4 $Na_2SO_{4(S)}$ $Na_2SO_{4(ii)}$ $Na_2SO_{4(iii)}$ $Na_2SO_{4(iv)}$ $Na_2SO_{4(v)}$ NaCl $NaCl_{(S)}$ NaOH $Na_2O.SiO_2$ $(Na_2O.SiO_2)_2$ $Na_2O.SiO_{2(S)}$ $(Na_2O.SiO_2)_{2(S)}$
S	S $S_{(S)}$ H_2S SN SO COS SO_2 SO_3 S_2
Cl	HCl CCl CCl_2 CCl_3 CCl_4 C_2Cl_6 Cl ClO Cl_2
Si	$Si_{(S)}$ Si Si_2 Si_3 $SiO_{2(S)}$ Si_2O_4 SiCl $SiCl_2$ $SiCl_2H_2$ $SiCl_3$ $SiCl_3H$ $SiCl_4$ SiH SiH_4

The equilibrium calculations are sensitive to the elemental composition of the system [27], therefore different cases were considered for comparison. $K_2CO_{3(S)}$, $K_2SO_{4(S)}$, K_2O-$(SiO_2)_{(S)}$ and $KCl_{(S)}$ were chosen as the initial solid state of potassium and Na_2O-$(SiO_2)_{(S)}$, $Na_2SO_{4(S)}$ and $NaCl_{(S)}$ were considered for sodium. Different concentrations have been tested and the results are found not sensitive to the initial concentrations of these compounds.

Three different cases were considered; in Case I, the main solid form was represented by $C_{(S)}$, in Case II, 10% (mass base) of moisture was added to $C_{(S)}$ and in Case III, the solid biomass was approximated by $C_6H_{10}O_5$ in the presence of H_2O. The pressure of the system was set to 1 bar and the temperature was varied from 500 to 1500 K. The main species of potassium and sodium from equilibrium calculations for the three cases are presented in Figure 6. Comparing the results of Case I and II shows that in the presence of water vapor the main potassium and sodium compound changes from K and Na to KOH and NaOH, respectively. By adding H_2O to the system, $K_2CO_{3(S)}$ and $KCl_{(S)}$ become stable until higher temperatures and the amount of KCl in the gas phase is reduced by an order

of magnitude. In the temperature range of 500 to 1000, the equilibrium mole fraction of $K_2CO_{3(S)}$ shows a 50% increase and the equilibrium mole fraction of $KCl_{(S)}$ shows up to 100% increase in comparison with their initial values. This increase can indicate that during the pyrolysis stage, evaporated inorganic potassium can be redeposited in the solid structure in the form of $K_2CO_{3(S)}$ and $KCl_{(S)}$. This is in agreement with the findings of Jensen et al. [11]. For sodium release, on the other hand, the evaporation of $NaCl_{(S)}$ is dominant and part of the evaporated inorganic sodium is redeposited in the form of Na_2O-$SiO_{2(S)}$ and remains stable until high temperatures.

For Case III, the results are fairly different. KOH is the main gaseous species of potassium. For sodium, NaOH, NaCl and Na are presented in the gas phase but in a considerably lower concentrations compared with case I and II.

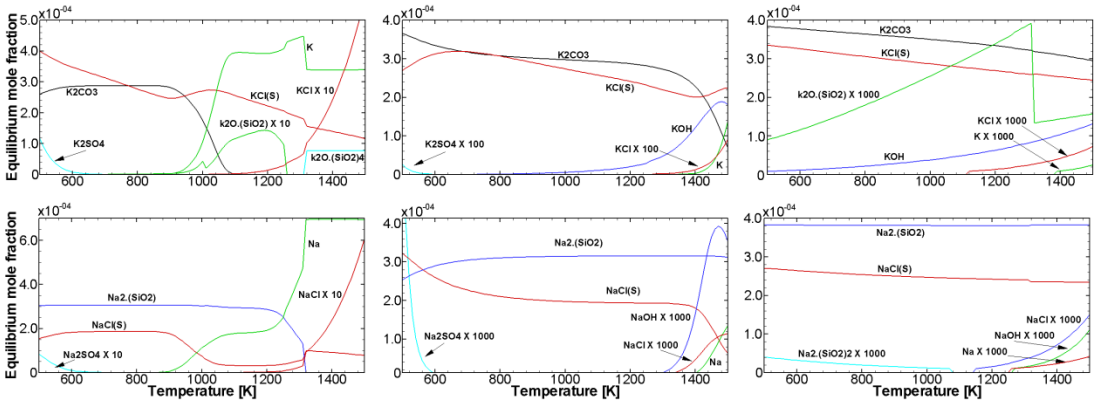

Case I Case II Case III

Figure 6. Main species of potassium and sodium from equilibrium calculations of three different cases

It should be noted that for large particles, different parts of the particle can be in different stages of thermochemical conversion. The overlapping between different processes indicates that char, biomass and water vapor can coexist in the particle; char at the outer part, dry biomass in the middle part and moist biomass at the center of the particle. Thus, the overall release of potassium and sodium to the gas

phase can be considered as the sum of the results from Case I to III. By considering these three cases, one can conclude that at low temperature the main potassium species in the gas phase is KOH, while at moderate temperatures atomic K can be dominant. At higher temperature, towards the end of the pyrolysis, KCl can be released to the gas phase. Atomic sodium, Na, and at higher temperatures with lower concentrations NaOH and NaCl are the main sodium species in the gas phase.

5. Conclusion

The release of potassium and sodium from a biomass particle during pyrolysis stage were experimentally and numerically studied. The experiments were carried out using the LIBS technique, a powerful atomic spectroscopic method that can overcome the laser scattering during the pyrolysis stage. The results showed distinct behaviors during the pyrolysis and gasification stages, indicating different mechanisms and kinetic rates for the release of alkali metals at these stages. The experimental measurements were used to extract the global kinetic constants of alkali metals release during the pyrolysis stage. To find the kinetic constants, the temperature at the potassium and sodium "reaction front" is required. Due to the high spatial variations of temperature inside the particle, a detailed particle model was employed to assign corresponding temperature to the release rates. The average activation energy for the release of sodium was found to be $223\ kJ/mole$ and for potassium $185\ kJ/mole$. The kinetic data could predict the amount of potassium and sodium released during the pyrolysis stage. It was shown that during the pyrolysis stage up to 55% of the sodium and less than 10% of potassium was released. To investigate the composition of sodium and potassium compounds in the gas phase, thermodynamic equilibrium calculations were carried out in the temperature range of 500 to 1500 K. Three cases were considered, representing large particles during the pyrolysis stage. Due to the overlapping processes in large particles, char, water vapor and biomass can coexist and different

potassium and sodium compounds can be originated from these different parts. By analyzing these different cases, the stable sodium and potassium compounds in the gas phase were discussed.

Acknowledgment

This work was financially supported by the Swedish Energy Agency (STEM) through CECOST and Swedish–Chinese Collaboration Project and the ERC Advanced Grant "TUCLA".

References

1. H. Schürmann, P.B. Monkhouse, S. Unterberger, K.R.G. Hein, Proc. Combust. Inst. 31(2) (2007) 1913-1920.
2. J.M. Jones, L.I. Darvell, T.G. Bridgeman, M. Pourkashanian, A. Williams, Proc. Combust. Inst. 31(2) (2007) 1955-1963.
3. B. PetersJ. Smuła-Ostaszewska, Fuel 96 (2012) 29-42.
4. X. Wei, U. Schnell, K.R.G. Hein, Fuel 84(7–8) (2005) 841-848.
5. L. Lisi, G. Lasorella, S. Malloggi, G. Russo, Appl. Catal. B: Environ. 50(4) (2004) 251-258.
6. H. Fatehi, Y. He, Z. Wang, Z.S. Li, X.S. Bai, M. Aldén, K.F. Cen, Proc. Combust. Inst. 35(2) (2015) 2389-2396.
7. P.J. van Eyk, P.J. Ashman, G.J. Nathan, Combusti. Flame 158(12) (2011) 2512-2523.
8. V. Doshi, H.B. Vuthaluru, R. Korbee, J.H.A. Kiel, Fuel Proces. Tech. 90(9) (2009) 1148-1156.
9. T. Khazraie Shoulaifar, N. DeMartini, M. Zevenhoven, F. Verhoeff, J. Kiel, M. Hupa, Energy Fuels 27(10) (2013) 5684-5690.
10. S.B. Saleh, J.P. Flensborg, T.K. Shoulaifar, Z. Sárossy, B.B. Hansen, H. Egsgaard, N. DeMartini, P.A. Jensen, P. Glarborg, K. Dam-Johansen, Energy Fuels 28(6) (2014) 3738-3746.
11. P.A. Jensen, F.J. Frandsen, K. Dam-Johansen, B. Sander, Energy Fuels 14(6) (2000) 1280-1285.
12. E. Björkman, B. Strömberg, Energy Fuels 11(5) (1997) 1026-1032.
13. M.U. Rahim, X. Gao, H. Wu, Proc. Combust. Inst. 35(3) (2015) 2891-2896.
14. J.N. Knudsen, P.A. Jensen, K. Dam-Johansen, Energy Fuels 18(5) (2004) 1385-1399.

15. D.J. Lane, P.J. van Eyk, P.J. Ashman, C.W. Kwong, R. de Nys, D.A. Roberts, A.J. Cole, D.M. Lewis, Energy Fuels 29(4) (2015) 2542-2554.

16. J.M. Johansen, M. Aho, K. Paakkinen, R. Taipale, H. Egsgaard, J.G. Jakobsen, F.J. Frandsen, P. Glarborg, Proc. Combust. Inst. 34(2) (2013) 2363-2372.

17. J.M. Johansen, J.G. Jakobsen, F.J. Frandsen, P. Glarborg, Energy Fuels 25(11) (2011) 4961-4971.

18. P.J. van Eyk, P.J. Ashman, Z.T. Alwahabi, G.J. Nathan, Combust. Flame 158(6) (2011) 1181-1192.

19. Z. h. Zhang, Q. Song, Z.T. Alwahabi, Q. Yao, G.J. Nathan, Combust. Flame 162(2) (2015) 496-505.

20. H. Fatehi, X.S. Bai, Combust. Sci. Tech. 186(4-5) (2014) 574-593.

21. R.B. Bird, W.E. Stewart, E.N. Lightfoot, Transport phenomena, New York (1960), John Wiley and Sons.

22. F. Frandsen, K. Dam-Johansen, P. Rasmussen, Prog. Energy Combust. Sci. 20(2) (1994) 115-138.

23. CHEMKIN-PRO, Reaction Design. 2013, San Diego.

24. E. Goos, A. Burcat, B. Ruscic, Thermodynamic Database, 2015.

25. P. Glarborg, P. Marshall, Combust. Flame 141(1–2) (2005) 22-39.

26. M.D. Allendorf, K.E. Spear, Journal Electrochemical Society 148(2) (2001) B59-B67.

27. P.F.B. Hansen, K.H. Andersen, K. Wieck-Hansen, P. Overgaard, I. Rasmussen, F.J. Frandsen, L.A. Hansen, K. Dam-Johansen, Fuel Proc. Tech. 54(1–3) (1998) 207-225.